

EVOLVING PHOTOSPHERIC FLUX CONCENTRATIONS AND FILAMENT DYNAMIC CHANGES

B. SCHMIEDER, G. AULANIER, and P. MEIN

*Observatoire de Paris, Laboratoire d'Etudes Spatiales et d'Instrumentation en Astrophysique,
F-92195 Meudon Cedex, France
(e-mail: brigitte.schmieder@obspm.fr)*

and

A. LÓPEZ ARISTE

THEMIS, CNRS UPS 853, Via Lactea, 38200 La Laguna, Tenerife, Spain

(Received 29 June 2006; accepted 7 September 2006; Published online 8 November 2006)

Abstract. We analyze the role of weak photospheric flux concentrations that evolve in a filament channel, in the triggering of dynamic changes in the shape of a filament. The high polarimetric sensitivity of THEMIS allowed us to detect weak flux concentrations (few Gauss) associated with the filament development. The synoptic instruments (MDI, SOLIS) even if their sensitivity is much less than THEMIS were useful to follow any subsequent strengthening of these flux concentrations after their identification in the THEMIS magnetograms. We found that (1) the northern part of the filament develops an $H\alpha$ barb at the same time that weak minority polarity elements develop near a plage; (2) a section in the southern part of the $H\alpha$ filament gradually disappears and later reforms at the same time that several mixed-polarity magnetic elements appear, then subsequently cancel or spread away from each other. These changes correspond to increases in EUV emission, as observed by TRACE, EIT, and CDS. This suggests that the plasma is temporarily heated along the filament spine. An idealized sequence of force-free models of this filament channel, based on plasma-supporting magnetic dips occurring in the windings of a very weakly twisted flux tube, naturally explains the evolution of its southern part as being due to changes in the topology of the coronal magnetic field as the photospheric flux concentrations evolve.

1. Introduction

Magnetic field plays a key role in prominence formation and evolution, due to the low plasma β in these structures (10^{-3} to 10^{-1}). It supports the prominence against gravity, whose plasma is 100 times denser than the coronal plasma. It also channels both plasma motions and thermal conduction and plays an important role in prominence eruptions. Filaments are always located within filament channels, which are broad corridors nearly free of magnetic flux, apart from some small, dispersed, flux concentrations (see *e.g.*, Martin, 1998; Chae *et al.*, 2001). Small-scale magnetic changes in these flux concentrations, such as their emergence and cancellation, have frequently been reported a few hours prior to local filament restructuring (*e.g.*, Chae *et al.*, 2000; Deng *et al.*, 2002; Wood and Martens, 2003).

The role of photospheric flux concentrations in either type of filament restructuring is particularly important when they occur in magnetic polarities close to the sites of linkage between successive sections of one (or several) filament(s), such as the so-called feet/legs/barbs (*e.g.*, Martens and Zwaan, 2001).

On one hand, according to observations and models, filament feet are associated with flux concentrations whose magnetic polarity is of the opposite sign as that of the background polarity on the side of the inversion line where they are located (Martin, Bilimoria, and Tracadas, 1994; Aulanier *et al.*, 1998). These parasitic polarities may be responsible for the formation of plasma-supporting magnetic dips within the feet, as initially proposed in the models of Aulanier and Démoulin (1998) and recently supported by spectro-polarimetric observations (López Ariste *et al.*, 2006). The motion of such a parasitic polarity has been related with the evolution of a filament foot within one day (Aulanier *et al.*, 1999).

On the other hand, the displacement of small flux concentrations of the same polarity as the background are also important in the dynamical restructuring of the filaments, as modeled by Aulanier, DeVore, and Antiochos (2006) and as clearly observed by Deng *et al.* (2002). Martin *et al.* (1985, 1998) established that the apparent mutual cancelation of such non-parasitic patches, originating from both sides of the large-scale inversion line and so having opposite polarities, is strongly correlated with the formation of filaments. The models of van Ballegoijen and Martens (1989) showed that such flux cancelation can lead to a restructuring of the magnetic field, resulting, in the formation of helical flux tubes containing plasma-supporting magnetic dips. Martens and Zwaan (2001) extended these previous 2.5D models to more realistic 3D configurations, in which flux cancelation can lead to the formation of new filaments or filament linkage. Many observations supported this view (Deng *et al.*, 2002; Wood and Martens, 2003; Schmieder *et al.*, 2004; Chae, Moon, and Park, 2005).

In spite of these numerous past studies, several questions remain unanswered, due to both observational and theoretical limitations. Observationally, the analysis of the magnetic-flux evolution was limited due to polarimetry sensitivity and time cadence of the instruments, so that the association between an observed cancelation event could not be unambiguously related with a filament restructuring event. Theoretically, most models assumed large-scale flux motions around filament inversion lines – rarely the evolution of isolated flux concentrations.

In this paper, we focus on two non-eruptive filament restructuring episodes (the formation of a foot and the transient interruption of the spine), which we study with a sequence of several magnetographs obtained during an international campaign, in conjunction with an idealized model whose boundary conditions mimic the observed flux concentrations. In Section 2, we present multi-wavelength observations, with an emphasis on the THEMIS magnetographic data. The high magnetic sensitivity of THEMIS enables us to detect very-weak magnetic polarities (a few

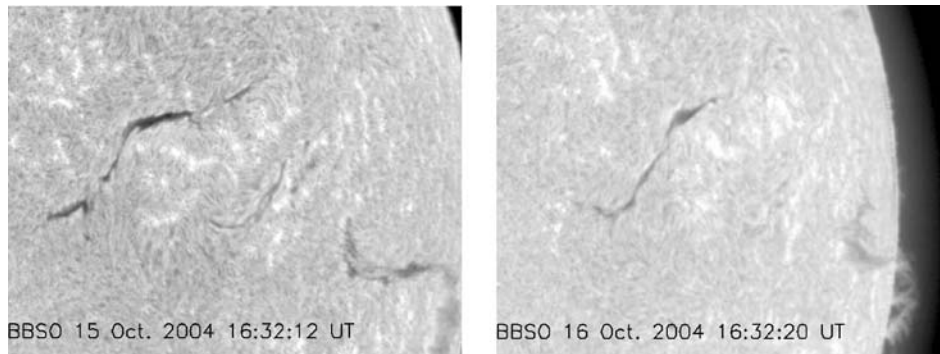


Figure 1. $H\alpha$ observations at BBSO of a filament (*left panel*) on October 15, 2004, at 16:32 UT and (*right panel*) on October 16, 2004, at 16:32 UT. We recognize the general shape of the filament and its fine structures between these two observations 24 hours apart.

$\text{Mx}\cdot\text{cm}^{-2}$ or Gauss¹) in filament channels (López Ariste *et al.*, 2006). The evolution of weak flux concentrations and transient changes in the filament are there directly related with unprecedented detail and confidence. THEMIS being capable of simultaneous multi-line observations, no co-alignment procedures were required to achieve such results. We further propose a physical interpretation based on a sequence of idealized, linear, force-free-field models, which explains the reconnection between field lines from the flux concentrations and the main flux tube supporting the filament (Section 3). We conclude that the interruption and the reformation of parts of the filament, as observed in $H\alpha$, can be interpreted as consequences of this reconnection process, which is independently supported by evidence of plasma heating all along the filament spine as observed in the EUV.

2. Observations

2.1. COORDINATED OBSERVATIONS

Joint Observing Program (JOP) 178 allowed us to follow the changes of a filament for two days, on October 15 – 16, 2004. The filament was located approximately at N10E27 on October 15, 2004; it spanned over 15° in longitude and 8° in latitude (see Figure 1). Synoptic spectroheliographs obtained from the Meudon and Big Bear observatories provided the daily evolution of the filament in $H\alpha$. The Meudon

¹Magnetographs measure longitudinal flux density, which is given in units of $\text{Mx}\cdot\text{cm}^{-2}$. If the magnetic field is homogeneous over the resolution element, a flux density of $1 \text{ Mx}\cdot\text{cm}^{-2}$ corresponds to a field strength of 1 G. Since this is not the case in general in the solar photosphere, G and $\text{Mx}\cdot\text{cm}^{-2}$ are not equivalent units. Nevertheless, the literature quotes uniquely G as unit of measure for magnetograph instruments such as MDI, creating confusion between flux measurements and field-strength determinations.

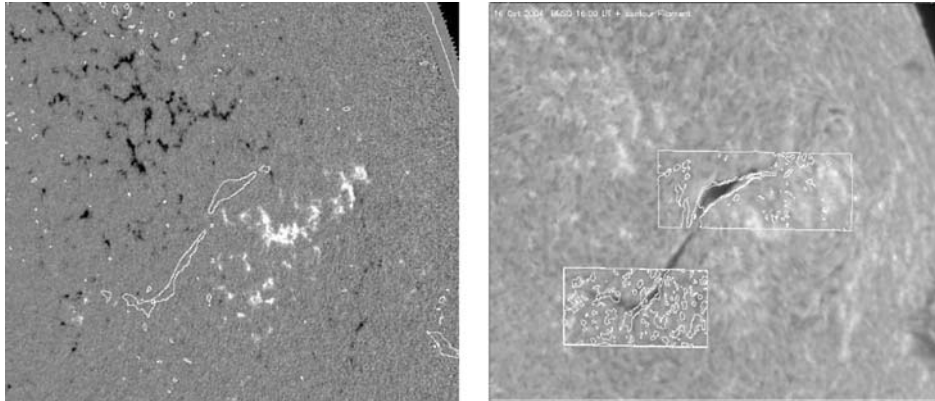


Figure 2. MDI magnetogram overlaid by the $H\alpha$ filament contour on October 16, 2004, at 16:00 UT (*left*) and BBSO $H\alpha$ image centered on the filament (*right*) overlaid by the two field-of-views of THEMIS/MSDP observations (north and south sections).

spectrograph provided full-disk images in five wavelengths in the $H\alpha$ line ($\pm 1 \text{ \AA}$, $\pm 0.5 \text{ \AA}$, center). The wing images obtained at 12:24 UT show different patterns that we interpreted as due to large Doppler shifts. These velocities could be associated with the important changes in the structure of the filament on October 16, 2004. TRACE also observed the filament with a high cadence of 30 seconds in white light, 1600, and 1700 \AA and with a slower cadence in 171 \AA . On October 16 only, the CDS instrument onboard SoHO ran in the so-called raster mode, covering an area of $240'' \times 240''$ in six spectral lines: Si XII 521.27 \AA , O IV 554.40 \AA , Ca X 558.48 \AA , Fe XIX 592.77 \AA , Mg X 625.04 \AA , and O IV 629.15 \AA . SoHO/MDI observed this region with a fast cadence of one minute, in its low-spatial-resolution mode (1.96'' per pixel) (see Figure 2). Finally, the SVM instrument of the SOLIS ground-based telescope also provided magnetographic data, during the two days of observations.

2.2. SPECTRO-POLARIMETRIC OBSERVATIONS

The spectro-polarimetric observations were made with the THEMIS telescope at the Observatorio del Teide at Izaña, in two different instrumental modes on October 16, 2004: the MSDP spectro-imaging instrument used two cameras sequentially for the $H\alpha$ line at 6563 \AA and for the Na D₁ line at 5896 \AA ; the multi-line spectrograph MTR simultaneously recorded three spectral domains comprising the $H\alpha$ line, the Na D₁ line, and the Fe I doublet at 6301 and 6302 \AA respectively. THEMIS is a polarization-free telescope designed specially for high-precision polarimetric observations.

In its MTR instrumental mode, the simultaneous observations in several spectral lines with different formation heights probe the solar atmosphere from the low photosphere to the chromosphere. By default, the MTR mode results in full vector polarimetry which, in appropriate spectral lines, results in determination of the

magnetic-field vector. For the purpose of our paper, we present here only the results concerning the longitudinal magnetic field. The data reduction was done with the SQUV package provided by THEMIS (Sainz Dalda and López Ariste, 2006). The vector magnetic field has been analyzed in detail in a previous work (López Ariste *et al.*, 2006). In this MTR mode, two fields were scanned: the north section covered an area of $240'' \times 105''$ in 2.5 hours, the south section an area of $96'' \times 105''$ was scanned in 1.25 hours. For both regions, the pixel size along the slit was $0.45''$, and the scans were performed with a step of $0.8''$, for a slit width of $0.5''$.

On the other hand, the MSDP instrumental mode provides the longitudinal magnetic field over a large field-of-view in a shorter time than the MTR mode. A detailed description of the specific instrumental setup of THEMIS in the MSDP mode is given by Mein (2002). The calibration of the MSDP magnetic field has been checked against MDI by Berlicky, Mein, and Schmieder (2006). There is good agreement for magnetic fluxes between 100 and $400 \text{ Mx} \cdot \text{cm}^{-2}$. At any rate, the sensitivity of THEMIS, even with our setup, is much higher than that of MDI, and weak field fluxes corresponding to two G can be detected with high confidence (López Ariste *et al.*, 2006).

In Figure 3, we present an example of the THEMIS/MSDP observation on October 16, 2004. The fields-of-view of the MSDP are slightly wider than the MTR fields-of-view. The top images concern the MSDP observations of the northern section of the filament ($100'' \times 250''$) obtained in roughly 20 minutes for each line. The figures show reconstructed maps at the $H\alpha$ line center (chromosphere) and the longitudinal magnetic field computed from the Na D₁ line (at $\pm 0.24 \text{ \AA}$ from the line center).

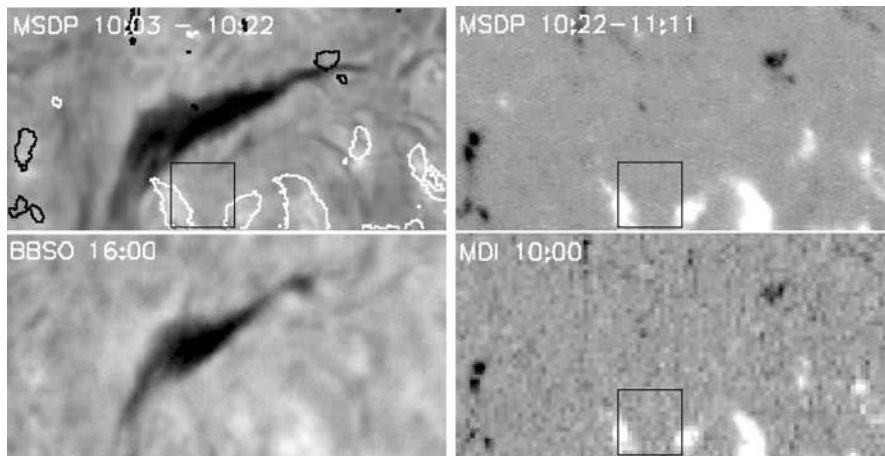


Figure 3. Northern part of the filament ($H\alpha$) and filament channel (magnetic field) observed with THEMIS/MSDP, MDI, and BBSO. The box (that will be referred to as A) corresponds to the location of a small emerging bipole which will be visible later at 14:00 UT and with no $H\alpha$ absorption (see next figure). The grey-scale rendering for magnetic flux saturates at $\pm 15 \text{ G}$ for the MSDP and $\pm 100 \text{ G}$ for MDI.

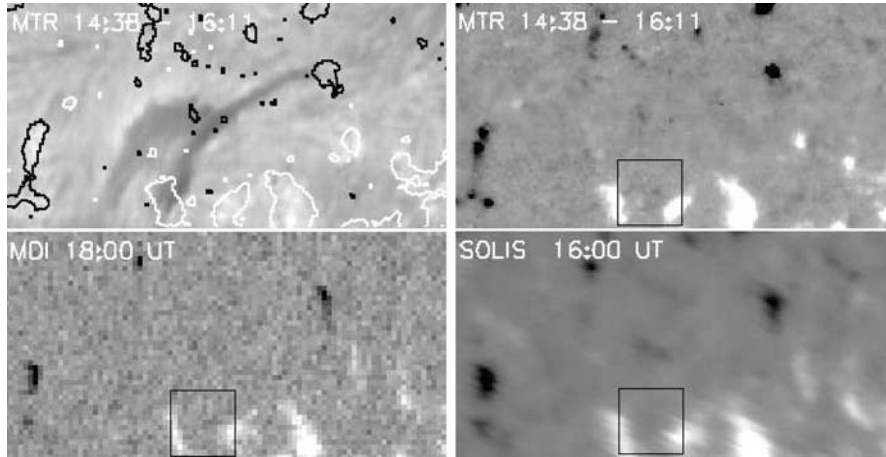


Figure 4. Northern part of the filament ($H\alpha$) and filament channel (magnetic field) observed with THEMIS/MTR, MDI, and SOLIS. The box (A) corresponds to the location of small emerging bipoles visible at 16:00 UT in the MTR observations and a barb as the counterpart in $H\alpha$. The grey-scale rendering for magnetic flux saturates at ± 20 G for MTR and ± 150 G for MDI.

3. Observational Results

3.1. EMERGING AND CANCELING FLUX

Figures 3 – 6 show the changes of the $H\alpha$ filament pattern on October 16, 2004. The northern section of the filament (Figures 3 and 4) looks relatively similar at 10:00 UT (MSDP) and at 16:00 UT (BBSO). Between these two times, the filament underwent some changes with the appearance of an additional structure. The new structure is a long, lateral, $H\alpha$ barb extended in the North – South direction (MTR in Figure 4). The filament change corresponds to the evolution of the magnetic field enclosed in the box drawn in Figures 3 and 4 and that we called A. In the MTR magnetogram (between 14:30 and 16:11 UT) small negative minority polarities are detected close to the positive polarity at box A. Neither MDI nor THEMIS/MSDP magnetograms show such minority polarities (negative) around 10:00 UT. These polarities are nevertheless difficult to see both in MDI and in SOLIS magnetograms because of the low, magnetic sensitivity of these instruments. However, the MSDP could have detected them if they were present at the time, as is demonstrated for the south section. We therefore conclude that the barb in A is related to the emergence of the observed negative polarity.

The southern part of the filament partly vanished during the MSDP observations and is replaced by a round-shaped brightening in $H\alpha$ enclosed in box B (08:48 – 09:07 UT) (Figures 5 and 6). The counterpart of the $H\alpha$ brightening is a ring of small and weak polarities in the MTR magnetogram. These polarities are well

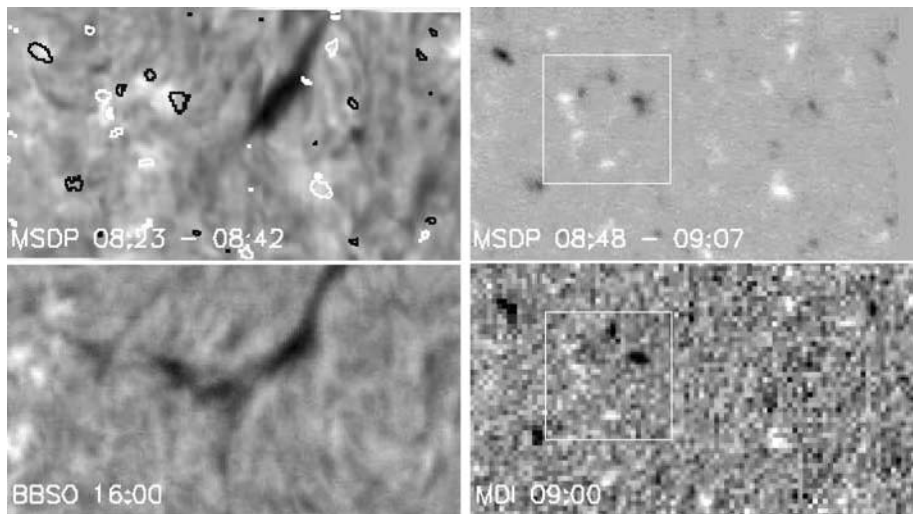


Figure 5. Southern part of the filament ($H\alpha$) and filament channel (magnetic field) observed with THEMIS/MSDP, MDI, and BBSO. Notice in the box (referred to as *B*) the presence of weak polarities corresponding to a bright ring in $H\alpha$ and no filament section (*top left panel*). The grey-scale rendering for magnetic flux saturates at ± 15 G for MSDP and ± 100 G for MDI.

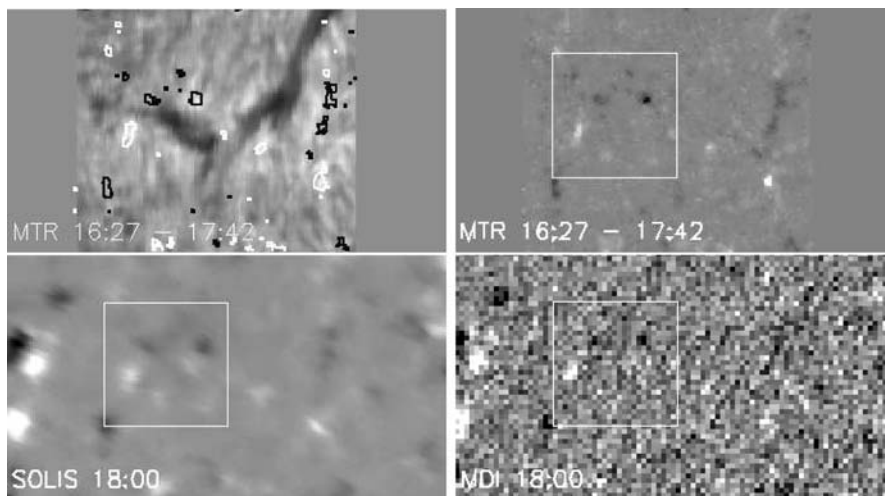


Figure 6. Southern part of the filament ($H\alpha$) and filament channel (magnetic field) observed with THEMIS/MTR, MDI, and SOLIS. Notice the decrease in the number of magnetic elements found in box *B* of the THEMIS/MTR magnetogram at 17:00 UT and barely detectable in MDI at 18:00 UT, and the reforming $H\alpha$ filament section (*left top panel*). The grey-scale rendering for magnetic flux saturates at ± 20 G for MTR and ± 150 G for MDI.

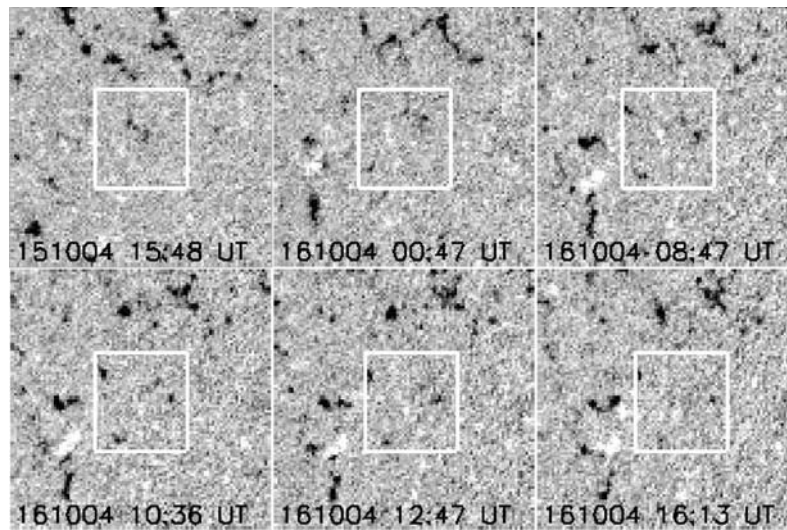


Figure 7. Emerging and canceling flux observed with MDI on October 16, 2004. The box indicates the region of interest (box B of Figure 6). Other emerging flux (left side of the box) occurs in the vicinity but does not interact with the filament. The grey-scale rendering for magnetic flux saturates at ± 100 G.

observed with THEMIS/MSDP as well, but are nearly completely buried in the noise of MDI data. Since these small polarities are in the large filament channel and along the inversion line where the background longitudinal field component is nearly zero, we could follow the evolution of these weak polarities in MDI despite its considerable noise. In particular, we study the evolution of the ring-shaped magnetic elements (Figure 7). The emergence of these magnetic elements occurs on October 15 at 15:48 UT. We see the enlargement of its diameter in the following frames on October 16 (at 00:47, 08:47, 10:36 UT). The polarities disappear later in the day and are very weak at 16:13 UT (Figure 7). These small polarities are nearly invisible in the MTR magnetogram between 16:27 and 17:42 UT (Figure 6). Figure 8 sketches the evolution of these small polarities. We identify six magnetic flux concentrations: three have positive polarities, three have negative polarities. They are found in a circular shape at 00:47 UT on October 16, as is commonly observed when new flux starts to emerge (Schmieder *et al.*, 2004). At 08:47 and 10:36 UT, two of these polarities are close to each other and merge before 12:47 UT. Then the polarities disperse.

In the MDI movie, we can see the evolution of this emerging flux, not visible until October 16 at 00:00 UT, developing until 09:00 UT, and progressively vanishing until 16:00 UT. The disappearance of the magnetic elements is interpreted as canceling flux from the small polarities approaching the secondary inversion line.

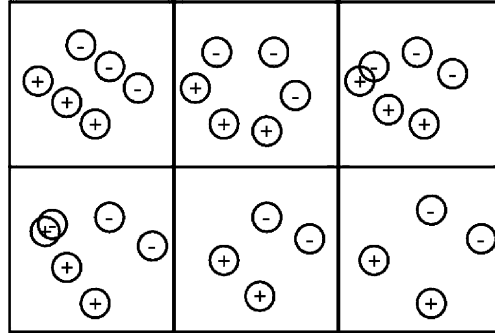


Figure 8. Small negative and positive polarities identified in Figure 7. The schematics frames are smaller than the *white boxes* in the magnetograms of Figure 7 in order to zoom in on the magnetic elements of interest.

3.2. HEATING ALONG THE FILAMENT SPINE

The changes in filament structures were accompanied by high $H\alpha$ Doppler shifts and heating of the plasma to transition-region and coronal temperatures (10^6 K) (see Figures 9 and 10). The whole spine of the filament is bright between boxes *A* and *B* in the CDS images, right from the beginning of the CDS observations at 10:17 UT, up to 12:22 UT (see Figure 11). Such EUV spine brightenings were already reported

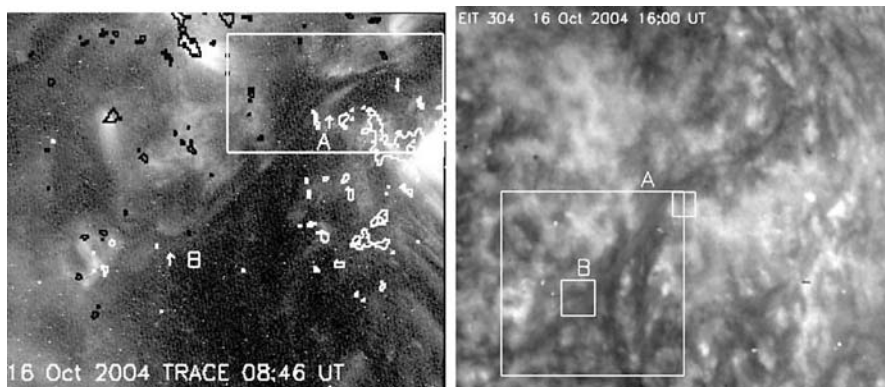


Figure 9. (*Left panel*) TRACE 195 Å image observed on October 16, 2004, at 08:46 UT overlaid by magnetic field contours of MDI (± 80 G) and a box corresponding to the north section of the filament in Figure 3. Notice the dark filament similar to the $H\alpha$ (Figure 1) surrounded by bright elongated structures between the points *A* and *B* pointed by *arrows*. (*Right panel*) EIT 304 Å image observed on October 16, 2004, at 16:00 UT enlarging elongated structure corresponding to the $H\alpha$ filament with short bright threads. The field-of-view of EIT is smaller than the TRACE one. The large box in the EIT image is the field-of-view of CDS ($240'' \times 240''$ in Figure 10). The two boxes *A* and *B* are drawn around the points *A* and *B* indicated on the TRACE image in the left frame. These boxes are the same as those represented in Figures 3 and 5.

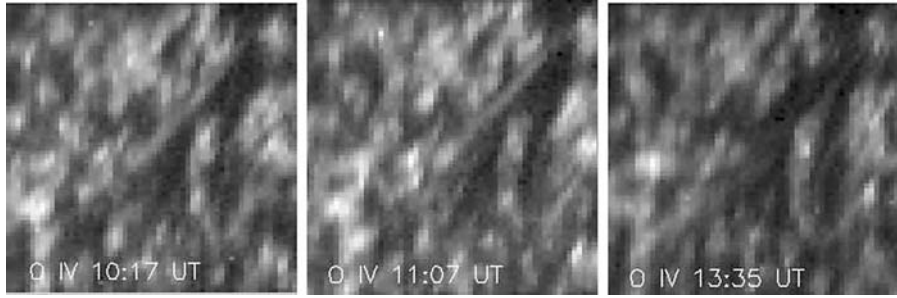


Figure 10. Change of brightness of the filament in O IV observed by CDS ($240'' \times 240''$). Notice the bright spine of the filament at 10:17 and at 11:07 UT following the first diagonal in the picture. The spine is no longer visible at 13:35 UT. At 11:07 UT, an additional bright point is visible in the southern part of the spine.

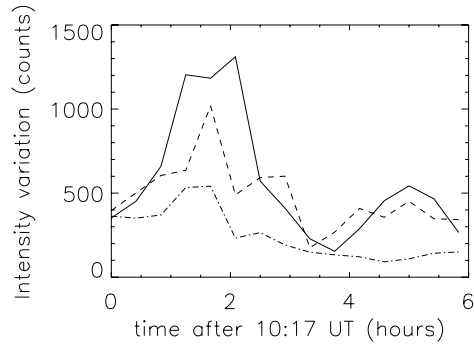


Figure 11. Evolution of the brightness at three different locations in the spine observed in O IV 554 Å. The *solid line* corresponds to the southern part of the spine where the variation could be due to flux cancelation. The common behavior of the three curves is the decrease of the brightness of the spine before 12:46 UT.

in Aulanier and Schmieder (2002) and have commonly been associated with strong activity along the filament (*e.g.*, Kucera *et al.*, 1999; Engvold *et al.*, 2001). The CDS images also show an enhancement of brightness in box *B*, corresponding to the disappearance of the bipole between 10:43 and 12:22 UT. This brightness is no longer visible in EUV lines later when the bipole vanishes and the filament reforms.

4. Linear Force-Free Field Modeling for the Filament Changes

So as to understand the role of the evolving photospheric flux concentrations in the dynamical changes that are observed in the southern part of the filament spine, we build a sequence of linear force-free field models, which satisfy

$$\nabla \times \mathbf{b} = \alpha \mathbf{b}, \quad (1)$$

where \mathbf{b} is the magnetic field, and α (= constant) is the force-free parameter. These models, further described below, incorporate two components: one that defines the filament and a second that is due to the flux concentrations. In all of these models, we fix the filament component, so the differences in the global configurations are solely due to the differences in the component that defines the photospheric flux concentrations.

The filament component is a 3D solution of the linear, force-free field equation (Equation (1)). It is the sum of a 2.5D field which defines a weakly-twisted flux tube invariant by translation along the filament axis (see Aulanier and Démoulin, 1998) and of two sub-photospheric charges (see Démoulin and Priest, 1992) which interrupt this flux tube at some point, so as to make the magnetic field fully 3D. In cartesian coordinates where (x, y) defines the photosphere (the y -axis is along the filament) and z -axis is the altitude in the corona, the magnetic field which defines the 2.5D flux tube is expressed as a linear combination of three Fourier modes, whose individual expressions are

$$b_x = -\frac{l_z m(n_x)}{k_x} \cos(k_x x) \exp(-l_z z), \quad (2)$$

$$b_y = -\frac{\alpha m(n_x)}{k_x} \cos(k_x x) \exp(-l_z z), \quad (3)$$

$$b_z = m(n_x) \sin(k_x x) \exp(-l_z z), \quad (4)$$

where α is the force-free parameter, and where $m(n_x)$ is the amplitude, $k_x = 2\pi n_x / l_x$ is the horizontal wavenumber, and $l_z = \sqrt{k_x^2 - \alpha^2}$ is the scale height of the mode n_x . The mode $n_x = 1$ defines the periodicity in the x direction: l_x . Choosing the parameters from the analysis of Aulanier and Démoulin (1998), the filament model here is defined using three modes: $m(1) = 10$, $m(2) = -7$, and $m(3) = 3$, with $l_x = 100$ Mm and $\alpha = 0.995 k_x \simeq 0.06$ Mm⁻¹. These values result in a weakly-twisted flux tube, in which plasma-supporting magnetic dips at $x = 0$ (*i.e.*, the filament spine) extend between $0 \text{ Mm} \leq z \leq 15 \text{ Mm}$. The photospheric vertical field ($b_z(z = 0)$) is bipolar, with a maximum amplitude of $\simeq 16$ G at $x = \pm 38$ Mm and with a broad filament channel located between $-20 \text{ Mm} \leq x \leq 20 \text{ Mm}$ that has a nearly-uniform weak vertical field of $\simeq 2$ G. Since the filament spine is not infinitely long toward the East (see Figures 1 and 6), two subphotospheric, linear, force-free magnetic sources with the same α are added to the Fourier modes to break the flux tube topology for low y values. The detailed expression of a source of intensity (C) and depth (d) below the photosphere is given in Démoulin and Priest (1992). The general effect of one source on the photosphere is the formation of a circular flux concentration of radius $R \simeq 2d$, with a vertical field that peaks at $b_z \simeq C/d^2$. The two sources are placed at $(x, y) = (\pm 40, -70)$ and they are characterized by $(C, d) = (\mp 4000, -20)$. These extended sources weakly modify the 2.5D field for $y < 20$, but the modifications are sufficient there to suppress the filament flux-tube topology, hence the magnetic dips. The upper-left panels of Figure 12 show full

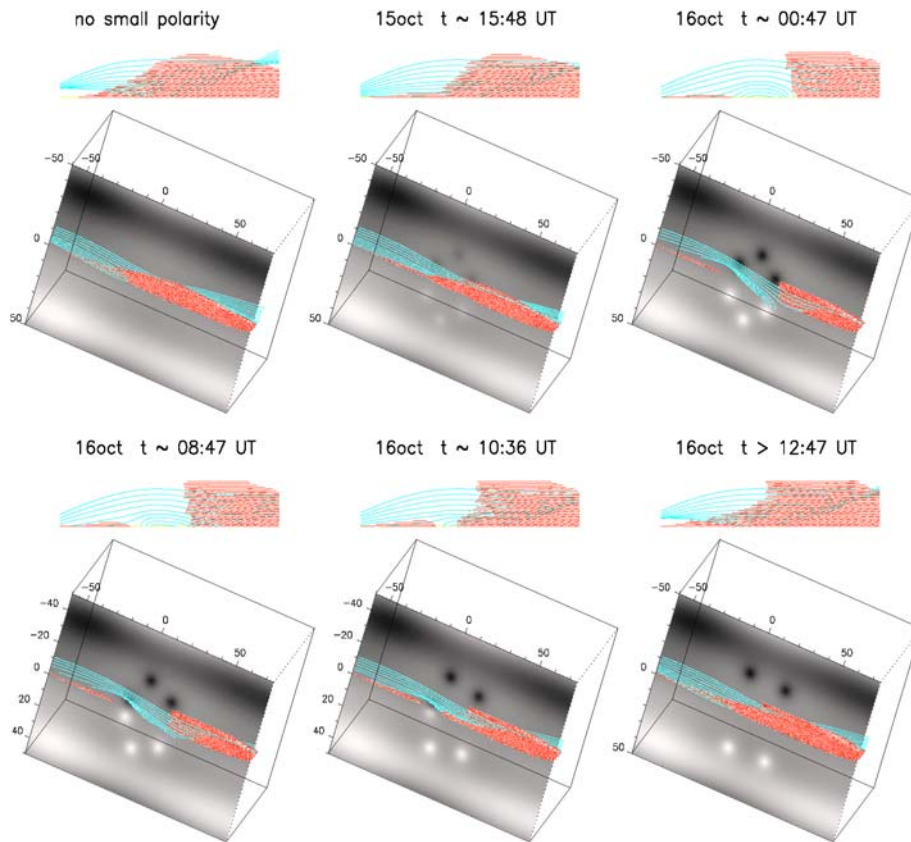


Figure 12. Sequence of linear force-free field models of the southern part of the filament. Each panel shows the models as viewed either from the side or from Earth. The grey-scale background stands for the vertical component of the photospheric magnetic field $b_z(z=0)$: white/black refers to $b_z(z=0) = \pm 20$ G. The cyan lines show a sample of full magnetic-field lines which pass above the photospheric inversion line $b_z(z=0) = 0$. The red segments show magnetic dips, which can support prominence plasma. These dips can simulate the filament observed in $H\alpha$.

field lines (in cyan) and magnetic dips (in red) drawn up to one pressure scale height (*i.e.*, 300 km), as viewed from the side and from Earth (taking into account the projection onto the solar disc). This method permits us to simulate $H\alpha$ observations of the filament spine (Aulanier *et al.*, 1998, 1999; Aulanier and Schmieder, 2002).

The filament magnetic-field component is perturbed by the inclusion of six subphotospheric sources. The positions in (x, y) and the parameters (C, d) of these sources are varied in five, independent, linear, force-free field models, accordingly to the general trends derived from the magnetographic observations reported in Figure 7 and summarized in Figure 8. These models are further ordered so as to simulate a time series (as done in Aulanier *et al.*, 1998, 1999 in which the time evolution of filament barbs was studied). For all five models, the depth of the six

sources is $d = 5$ Mm. For all four models of the filament observed on October 16, the intensities are $C = \pm 500$, with a $+$ ($-$) sign for $x > 0$ (< 0), so that their polarity is always of the same sign as that of the background bipolar field. Their maximum vertical field in the photosphere is therefore 20 G. For the model of October 15, during which the magnetic concentrations grew in flux, we use $C = \pm 150$. All these models are shown in Figure 12.

These magnetic models clearly are *ad hoc*: the ratio between the flux of the photospheric magnetic concentrations and that of the filament itself is still subject to uncertainties, and a sequence of independently calculated linear force-free fields cannot accurately represent a true MHD evolution. Nevertheless, these models capture most of the main properties of the southern part of the filament observed on October 15 and 16 (compare Figures 6, 7, 9, and 12): a part of the filament spine disappears in conjunction with the development of the photospheric flux concentrations, and it gradually reforms as some concentrations cancel with each other and as other spread away from the photospheric inversion line. Under the approximations of this model, the physical mechanism that is responsible for the dynamical changes observed in the filament spine must be magnetic reconnection between the evolving flux concentrations and the filament flux tube. Indeed, Figure 12 clearly shows that some (cyan) field lines, which are initially dipped and which do not join the photosphere on October 15 at 15:48 UT, change shape and start to form arcade-like connections between two flux concentrations on October 16 at 00:47 UT, which progressively turn back into filament-dipped field lines between 00:47 and 12:47 UT. Magnetic reconnection in the filament up to its top can account for the plasma heating which is observed in the EUV in the spine before the filament reforms.

5. Conclusion

We could identify the flux concentrations responsible for the changes of the $H\alpha$ filament pattern during 24 hours, with an unprecedented level of detail and confidence. Flux concentrations in the magnetograms as well as filament heating evolve relatively slowly: cancelation of small flux concentrations in the southern part of the filament takes two hours and the bright spine fades in more than two hours. The existence of a barb in the northern part of the filament occurs after the emergence of weak magnetic concentrations.

This study was possible due to the coordinated campaign performed on October 15 and 16, 2004. Small flux concentrations were detected by THEMIS, thanks to its high polarimetric sensitivity. Flux variations corresponding to two G could be observed with good confidence (López Ariste *et al.*, 2006), so that 20 G fluxes could undoubtedly be followed in time. The evolution of the magnetic and filament structures were also followed by synoptic instruments (MDI for the magnetic field, BBSO and Meudon spectroheliograms for the $H\alpha$ filament). The weak flux concentrations were still distinguishable in the MDI magnetograms despite the noise, because of the low value of the magnetic field in the filament channel.

Observationally, we associated the formation of a long barb, in the northern part of the filament, with the development of weak parasitic polarities on the edge of the filament channel. Also, we associated a transient and local interruption and reformation of the southern part of the filament spine with the emergence, cancelation, and spreading of a group of non-parasitic polarities in the middle of a filament channel.

An idealized sequence of force-free models of this filament channel, based on magnetic dips occurring in the windings of a very weakly twisted flux tube, has been developed for these observations. It explains the evolution of the southern part of the filament as being due to magnetic reconnection. The associated magnetic field restructuring first destroys and then reforms filament dips locally, around the flux concentrations. The wide range in altitude covered by this restructuring naturally accounts for the observed filament interruption and reformation. Both flux cancelation at the photospheric level and magnetic reconnection in the filament can account for the plasma heating which is observed in the EUV in this area.

Acknowledgments

The authors thank the THEMIS staff and the organizers of the JOP178 observing campaign, particularly Th. Roudier, in the framework of which this study has been performed. THEMIS is operated by the CNRS (France) and the INAF (Italy) on the Island of Tenerife (Spain). We used the THEMIS software developed by A. Sainz Dalda. This work was done in the framework of the RTN programme (European Solar Magnetism Network, contract HPRN-CT-2002-00313). We thank the staff of SAO and particularly J. Cirtain who provides the TRACE data. We thank Hui Li who produces the MDI movie. The authors would like to thank the referee, V. Gaizauskas, for his helpful comments that helped us to improve the manuscript.

References

- Aulanier, G. and Démoulin, P.: 1998, *Astron. Astrophys.* **329**, 1125.
Aulanier, G., Démoulin, P., van Driel-Gesztelyi, L., *et al.*: 1998, *Astron. Astrophys.* **335**, 309.
Aulanier, G., Démoulin, P., Mein, N., *et al.*: 1999, *Astron. Astrophys.* **342**, 867.
Aulanier, G. and Schmieder, B.: 2002, *Astron. Astrophys.* **386**, 1106.
Aulanier, G., DeVore, C.R., and Antiochos, S.K.: 2006, *Astrophys. J.* **646**, 1349.
Berlicki, A., Mein, P., and Schmieder, B.: 2006, *Solar Phys.* **445**, 1127.
Chae, J., Denker, C., Spirock, T., Wang, H., and Goode, P.R.: 2000, *Solar Phys.* **195**, 333.
Chae, J., Martin, S.F., Yun, H.S., Kim, J., Lee, S., Good, P.R., Spirock, T., and Wang, H.: 2001, *Astrophys. J.* **548**, 497.
Chae, J., Moon, Y.J., and Park, Y.D.: 2005, *Astrophys. J.* **626**, 574.
Démoulin, P. and Priest, E.R.: 1992, *Astron. Astrophys.* **258**, 535.
Deng, Y.Y., Lin, Y., Schmieder, B., and Engvold, O.: 2002, *Solar Phys.* **209**, 153.

- Engvold, O., Jakobsson, H., Tandberg-Hanssen, E., Gurman, J., and Moses, D.: 2001, *Solar Phys.* **202**, 293.
- Kucera, T., Aulanier, G., Schmieder, B., Mein, N., and Vial, J.C.: 1999, *Solar Phys.* **186**, 259.
- López Ariste, A., Aulanier, G., Schmieder, B., and Sainz Dalda, A.: 2006, *Astron. Astrophys.* **456**, 725.
- Martens, P.C. and Zwaan, C.: 2001, *Astrophys. J.* **558**, 872.
- Martin, S.F., Bilimoria, R., and Tracadas, P.W.: 1994, *NATO ASI Ser. C* **433**, 303.
- Martin, S.F.: 1998, *Solar Phys.* **182**, 107.
- Martin, S., Livi, S., and Wang, J.: 1985, *Aust. J. Phys.* **38**, 929.
- Mein, P.: 2002, *Astron. Astrophys.* **381**, 271.
- Sainz Dalda, A. and López Ariste, A.: 2006, *Astron. Astrophys.*, submitted for publication.
- Schmieder, B., Mein, N., Deng, Y.Y., Dumitrache, C., Malherbe, J.M., Staiger, J., and DeLuca, E.: 2004, *Solar Phys.* **223**, 119.
- Schmieder, B., Rust, D., Georgoulis, M.K., Démoulin, P., and Bernasconi, P.: 2004, *Astrophys. J.* **601**, 530.
- van Ballegoijen, A. and Martens, P.: 1989, *Astrophys. J.* **343**, 971.
- Wood, P. and Martens, P.: 2003, *Solar Phys.* **218**, 123.